ORGANOMETALLICS
Article
Cite This: Organometallics XXXX, XXX, XXX−XXX
pubs.acs.org/Organometallics

Half-Sandwich Ir(III) Complex of *N*1-Pyridyl-7-azaindole Exceeds Cytotoxicity of Cisplatin at Various Human Cancer Cells and 3D Multicellular Tumor Spheroids

Pavel Štarha,*[,†] Zdeněk Trávníček,[†] Hana Crlíková,[‡] Ján Vančo,[†] Jana Kašpárková,[‡] and Zdeněk Dvořák[†]

[†]Division of Biologically Active Complexes and Molecular Magnets, Regional Centre of Advanced Technologies and Materials, Faculty of Science, Palacký University, Šlechtitelů 27, 783 71 Olomouc, Czech Republic

[‡]Department of Biophysics, Faculty of Science, Palacký University, 17. listopadu 12, 771 46 Olomouc, Czech Republic

Supporting Information

ABSTRACT: The half-sandwich iridium(III) complexes [Ir(η^5-Cp^x)(*ph*aza$^-$)Cl] (**1**, **2**), [Ir(η^5-Cp^x)(*th*aza$^-$)Cl] (**3**, **4**), and [Ir(η^5-Cp^x)(*py*aza)Cl]PF$_6$ (**5**, **6**) containing deprotonated 1-phenyl-7-azaindole (*ph*aza$^-$) and 1-(thiophen-2-yl)-7-azaindole (*th*aza$^-$) and electroneutral 1-(pyridin-2-yl)-7-azaindole (*py*aza), were prepared; Cp^x = pentamethylcyclopentadienyl (Cp*; for **1**, **3**, and **5**) or 1,2,3,4-tetramethyl-5-phenylcyclopentadienyl (Cp^{ph}; for **2**, **4**, and **6**). The complexes were thoroughly characterized, including a single-crystal X-ray analysis of complexes **1**, **5**, and **6**. All of the complexes were screened for their in vitro cytotoxicity at the A2780 human ovarian carcinoma cell line and its A2780R cisplatin-resistant variant (2D culture cells). The best-performing complex **6** was further studied against the human DU-145 prostatic carcinoma, A549 lung carcinoma, HCT116 colon carcinoma, HeLa cervix adenocarcinoma, and MCF7 breast adenocarcinoma cell lines (2D culture cells). Complex **6** showed a cytotoxic profile different from that of cisplatin at the used cells, with the highest activity detected at the A2780, MCF7, and HCT116 cells (IC$_{50}$ = 3.1, 6.9, and 10.4 μM, respectively). Complex **6** exhibited relevant selectivity toward cancer cells (IC$_{50}$ = 3.1−13.0 μM) over the MRC-5 human noncancerous lung fibroblast cells (IC$_{50}$ > 50.0 μM). Complex **6** was markedly more accumulated by the A2780 cells in comparison to cisplatin after 24 h exposure. Flow cytometry studies showed that the cell cycle of the A2780 cells treated by complex **6** is modified differently (G$_0$/G$_1$ arrest) in comparison to cisplatin (G$_2$/M arrest). Additionally to the monolayer (2D) cancer cell cultures, the cytotoxicity of complex **6** was for the first time among half-sandwich iridium(III) complexes also assessed at spheroid (3D) MCF7 cells, where its potency (IC$_{50}$ = 22.9 μM for complex **6**) remained significantly better than that for the reference drug cisplatin (IC$_{50}$ = 35.4 μM).

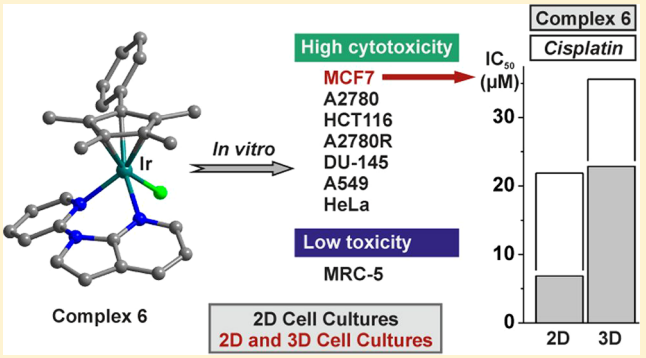

INTRODUCTION

Because of the known drawbacks (limited number of treatable tumors, intrinsic and acquired resistance, negative side effects, intravenous application) of the conventional platinum-based anticancer chemotherapeutics (e.g., cisplatin),[1] the field of medicinal chemistry faces a continual demand for substances overcoming these limitations. One of the most prospective groups of compounds includes organometallic complexes of non-platinum precious metals.[2] Among these compounds, iridium(III) half-sandwich cyclopentadienyl complexes were recently reported to be highly cytotoxic,[3] acting through a redox-mediated mechanism of action (MoA) different from the platinum-based drugs used in clinics.[3b,4] Concerning the structure−activity relationship of cytotoxic cyclopentadienyl iridium(III) complexes,[3−5] it was reported that ionic complexes containing electroneutral N,N-donor ligands such as [Ir(η^5-Cp*)(bpy)Cl]PF$_6$ (IC$_{50}$ > 100 μM) and [Ir(η^5-Cp^{ph})(bpy)Cl]PF$_6$ (IC$_{50}$ = 15.9 μM) are markedly less potent than the electroneutral analogues [Ir(η^5-Cp*)(phpy)Cl] (IC$_{50}$ = 10.8 μM) and [Ir(η^5-Cp^{ph})(phpy)Cl] (IC$_{50}$ = 2.1 μM), containing isoelectronic anionic C,N-coordinated ligands[6] (bpy = 2,2′-bipyridine, Hphpy = 2-phenylpyridine, Cp* = pentamethylcyclopentadienyl, Cp^{ph} = 1,2,3,4-tetramethyl-5-phenylcyclopentadienyl); all of the cited IC$_{50}$ values are associated with the A2780 human ovarian carcinoma cell line. Further, complexes with extended cyclopentadienyl ligands (e.g., Cp^{ph}) showed considerably higher potency in comparison to their Cp* analogues.[3b,5c,7] Both approaches (i.e., C,N- vs N,N-ligands and Cp* vs Cp^{ph} complexes) were applied in this work.

Received: June 15, 2018

DOI: 10.1021/acs.organomet.8b00415
Organometallics XXXX, XXX, XXX−XXX

1*H*-Pyrrolo[2,3-*b*]pyridine (7-azaindole) is a biologically very interesting heterocyclic compound, whose derivatives[8] or platinum(II) or gold(I) complexes[9] were recently reported as highly active against diverse diseases by various research groups. Our recent research also proved that monodentately coordinated 7-azaindole C derivatives release from half-sandwich Ru(II) dichlorido complexes in water-containing solutions.[10] This is why we decided to prepare the N1-substituted 7-azaindole derivatives, in particular 1-phenyl-7-azaindole (*ph*aza),[11] 1-(pyridin-2-yl)-7-azaindole (*py*aza),[12] and 1-(thiophen-2-yl)-7-azaindole (*th*aza),[13] as prospective bidentate ligands for anticancer half-sandwich complexes (Figure S1). Regarding the transition-metal complexes containing these ligands, no complexes containing *ph*aza and *th*aza have been reported to date. As for *py*aza, several complexes were reported as containing this ligand bidentately coordinated to the metal center through the nitrogen atoms of both its pyridines (numbered N7 and N9 in this work). In particular, $[Cu(pyaza)(PPh_3)_2]BPh_4$,[14] $[Zn(pyaza)(ac)_2]$, $[Zn(pyaza)(mba)_2]$,[12] $[Pt(pyaza)(Ph)_2]$, and $[Pt(pyaza)(Me)_2]$[15] were previously reported in the literature, but none of them were studied in connection with any kind of biological activity (ac = acetate anion, mba = 2-methylbutyrate anion, Ph = phenyl, and Me = methyl).

This work deals with the preparation, thorough characterization, and studies of in vitro cytotoxicity of a series of the neutral $[Ir(\eta^5\text{-}Cp^x)(naza^-)Cl]$ (*naza* = *ph*aza for **1** and **2** or *th*aza for **3** and **4**) and cationic $[Ir(\eta^5\text{-}Cp^x)(pyaza)Cl]PF_6$ (**5** and **6**) iridium(III) complexes containing the aforementioned 7-azaindole derivatives as bidentate C,N (*ph*aza$^-$, *th*aza$^-$)- or N,N-donor ligands (*py*aza) (Cp^x = Cp* for **1**, **3**, and **5**, and Cp^{ph} for **2**, **4**, and **6**) (Figure 1). The best-performing complex, **6**, was, as the first half-sandwich iridium(III) complex, studied for its in vitro cytotoxicity at the spheroid (3D) cell culture, representing an advanced model for biocharacterization of pharmacologically prospective cytotoxic agents.

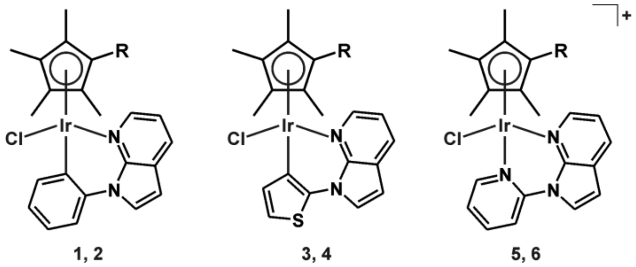

Complex	R
$[Ir(\eta^5\text{-}Cp^*)(phaza^-)Cl]$ (**1**)	CH_3
$[Ir(\eta^5\text{-}Cp^{ph})(phaza^-)Cl]$ (**2**)	Phenyl
$[Ir(\eta^5\text{-}Cp^*)(thaza^-)Cl]$ (**3**)	CH_3
$[Ir(\eta^5\text{-}Cp^{ph})(thaza^-)Cl]$ (**4**)	Phenyl
$[Ir(\eta^5\text{-}Cp^*)(pyaza)Cl]PF_6$ (**5**)	CH_3
$[Ir(\eta^5\text{-}Cp^{ph})(pyaza)Cl]PF_6$ (**6**)	Phenyl

Figure 1. Structural formulas and specification of composition of complexes **1**–**6**.

RESULTS AND DISCUSSION

Synthesis. A series of *ph*aza, *py*aza, and *th*aza 7-azaindole derivatives (Figure S1) was designed to obtain complexes containing bidentate 7-azaindole-based ligands coordinated differently to the Ir(III) metal center, in particular as C,N-, N,N-, and N,S-ligands, respectively. In the case of *ph*aza and *py*aza derivatives, the electroneutral complexes $[Ir(\eta^5\text{-}Cp^*)(phaza^-)Cl]$ (**1**) and $[Ir(\eta^5\text{-}Cp^{ph})(phaza^-)Cl]$ (**2**), containing the deprotonated C,N-coordinated *ph*aza$^-$ ligand, and the cationic complexes $[Ir(\eta^5\text{-}Cp^*)(pyaza)Cl]PF_6$ (**5**) and $[Ir(\eta^5\text{-}Cp^{ph})(pyaza)Cl]PF_6$ (**6**), containing *py*aza as the electroneutral bidentate N,N-donor ligand (Figure 1), were successfully prepared by syntheses using the dimeric complexes $[Ir(\mu\text{-}Cl)(\eta^5\text{-}Cp^*)Cl]_2$ and $[Ir(\mu\text{-}Cl)(\eta^5\text{-}Cp^{ph})Cl]_2$ as the starting Ir(III) compounds (Figure S2).

Concerning the *th*aza derivative, despite the fact that no base was added to the reaction mixtures, the electroneutral complexes $[Ir(\eta^5\text{-}Cp^*)(thaza^-)Cl]$ (**3**) and $[Ir(\eta^5\text{-}Cp^{ph})(thaza^-)Cl]$ (**4**) were prepared, containing *th*aza$^-$ as a deprotonated ligand coordinated through the N7 atom of the 7-azaindole moiety and C12 atom of the pendant thiophenyl group (see the Supporting Information for the atom-numbering scheme; Figure 1). Recently, it was described that the pendant thiophenyl ring of 3-(diphenylphosphane)-thiophene (P,C-ligand at alkaline pH) changes a P,C-coordination mode to a P,S-mode after the addition of trifluoroacetic acid (Htfa), which is accompanied by protonation of the appropriate carbon atom.[16] Indeed, subsequent addition of a base led to the reversion from P,S- to P,C-coordination mode. A similar phenomenon was reported for an iridium complex containing C,N-coordinated 2-(thiophene)ethaneimine, which reverted to the C,S-ligand with the addition of Htfa.[17] In the case of complexes **3** and **4** containing the C,N-coordinated *th*aza$^-$ ligand, a similar change from the observed C,N-coordination mode to the anticipated N,S-coordination mode was not detected by ^{1}H NMR even at pH ∼1 (the addition of Htfa).

General Characterization. The HPLC-MS results showed the purity of complexes **1**–**6** in methanolic solutions as 95.3–99.9% (Table S1) with a dominant chromatographic peak assigned to $[Ir(\eta^5\text{-}Cp^x)(naza^-)]^+$ for electroneutral complexes **1**–**4** (*naza*$^-$ = *ph*aza$^-$ or *th*aza$^-$), and to $[Ir(\eta^5\text{-}Cp^x)(pyaza)Cl]^+$ for cationic complexes **5** and **6**. A content of the dominant species detected by HPLC changed negligibly after 72 h of standing in MeOH at ambient temperature, where only complex **4** showed lower than 95% purity.

The ESI+ mass spectra (using direct injection without HPLC) of complexes **1**–**4** contained only one dominant peak (100% relative intensity) assignable to the dechlorinated species $[Ir(Cp^x)(naza^-)]^+$ (*naza*$^-$ = *ph*aza$^-$ or *th*aza$^-$; Figure S3). In contrast, the ESI+ mass spectra of the cationic complexes **5** and **6** showed two peaks assignable to the $[Ir(Cp^x)(pyaza)Cl]^+$ and $\{[Ir(Cp^x)(pyaza)] - H\}^+$ species.

All of the hydrogen atoms of cationic complexes **5** and **6** containing the electroneutral *py*aza ligand were detected by ^{1}H NMR spectroscopy (Figures S4–S6). In contrast, the ^{1}H NMR spectra of electroneutral complexes **1**–**4**, whose structures involve the deprotonated *ph*aza$^-$ and *th*aza$^-$ ligands, showed the appropriate ^{1}H NMR integral intensity decrease due to the mentioned deprotonation of the carbon coordination sites (i.e., C9 for *ph*aza$^-$ involved in complexes **1** and **2**, and C12 for *th*aza$^-$ involved in complexes **3** and **4**) during the complex formation (Figure 2). Regarding the ^{13}C and ^{15}N NMR spectra, all of the carbon and nitrogen atoms were detected for complexes **1**–**6**. A comparison of the spectra of the starting 7-azaindole derivatives with complexes **1**–**6** indirectly indicated the coordination sites of the used *naza* ligands. The ^{15}N NMR

DOI: 10.1021/acs.organomet.8b00415
Organometallics XXXX, XXX, XXX–XXX

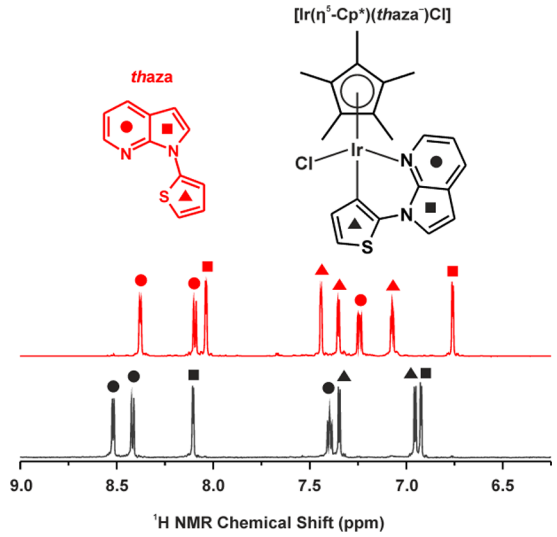

Figure 2. ^{1}H NMR spectra of free *th*aza (in red) and complex [Ir(η^5-Cp*)(*th*aza$^-$)Cl] (**3**), given with the general assignment of the detected aromatic hydrogen signals (all of the depicted signals have an integral intensity of ∼1).

coordination shifts ($\Delta\delta$) of N1, N7, and N9 of *py*aza are −1.9, −94.2, and −93.8 ppm for complex **5** and −2.9, −97.5, and −96.4 ppm for complex **6**. Similar ^{15}N NMR coordination shifts of N1 and N7 were detected for C,N-ligands *ph*aza$^-$ and *th*aza$^-$ contained in complexes **1** (−4.2 and −105.2 ppm), **2** (−11.8 and −104.5 ppm), **3** (−0.8 and −110.8 ppm), and **4** (−2.4 and −113.1 ppm) on N7-coordination of the mentioned *n*aza$^-$ ligands. A coordination of *ph*aza$^-$ and *th*aza$^-$ through the deprotonated C9 (for *ph*aza$^-$ of **1** and **2**) and C12 (for *th*aza$^-$ of **3** and **4**) carbon atoms was proved by the considerable ^{13}C NMR upfield shifts of the aforementioned atoms with $\Delta\delta$ values ranging from −35.4 to −10.2 ppm.

The characteristic peaks of the vibrations of the Cp^x ring were found in the FT-IR spectra of complexes **1**−**6** at ca. 2910−2970 cm^{-1} for ν_s(C−H) and ν_{as}(C−H) and at ca. 1450 and 800 cm^{-1} for ν_{as}(C−C) and ν_{as}(C−CH$_3$).[18] The spectra of the cationic complexes **5** and **6** contained a set of peaks of the ν(P−F) vibrations at 825, 770, and 555 cm^{-1}.[19]

X-ray Structures of Complexes 1, 5, and 6. The crystallographically characterized complexes **1**, **5**, and **6** adopt a piano-stool arrangement with a coordinated cyclopentadienyl ring, chlorido ligand, and a bidentate-bonded *n*aza ligand (Figure 3, Table 1, and Table S2).

The *ph*aza$^-$ ligand of complex **1** is coordinated through the N7 atom of the pyridine ring of the 7-azaindole moiety and the C9 atom of the pendant phenyl N1-substituent. Regarding

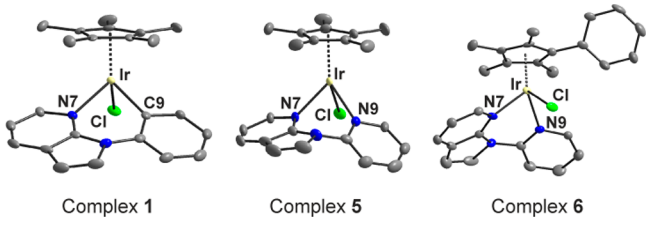

Figure 3. Molecular structures of complex **1** (left) and cations of complexes **5** (middle) and **6** (right). Hydrogen atoms (for **1**, **5**, and **6**) and PF_6^- anions (for **5** and **6**) are omitted for clarity and the non-hydrogen atoms are drawn as thermal ellipsoids at 50% probability.

Table 1. Selected Bond Lengths (Å) and Angles (deg) Determined by a Single-Crystal X-ray Analysis for Complexes 1, 5, and 6

	1	5	6
Bond Lengths (Å)			
Ir−N(7)	2.087(3)	2.028(3)	2.087(4)
Ir−C(9)	2.054(4)		
Ir−N(9)		2.158(3)	2.122(4)
Ir−Cl	2.4107(9)	2.4995(9)	2.3824(12)
Ir−C(20)	2.150(3)	2.314(4)	2.171(5)
Ir−C(21)	2.157(4)	2.341(4)	2.169(5)
Ir−C(22)	2.233(3)	2.209(4)	2.188(5)
Ir−C(23)	2.256(4)	2.278(4)	2.157(5)
Ir−C(24)	2.165(3)	2.306(4)	2.176(4)
Ir−Cg[a]	1.8207(2)	1.9710(3)	1.7886(5)
Bond Angles (deg)			
N(7)−Ir−C(9)	86.77(14)		
N(7)−Ir−N(9)		78.48(11)	82.5(2)
N(7)−Ir−Cl	88.91(9)	75.97(8)	87.06(11)
N(7)−Ir−Cg[a]	126.03(8)	132.26(8)	127.30(12)
C(9)−Ir−Cl	89.03(11)		
N(9)−Ir−Cl		82.33(8)	88.01(11)
C(9)−Ir−Cg[a]	127.78(9)		
N(9)−Ir−Cg[a]		129.91(8)	128.89(12)
Cl−Ir−Cg[a]	125.68(2)	135.98(2)	128.11(4)

[a]Cg = centroid of the cyclopentadienyl ring of the Cp* (for **1** and **5**) and Cp^{ph} (for **6**) ligands.

complexes **5** and **6**, the N7 (7-azaindole moiety) and N9 (pendant pyridine substituent) atoms were detected as the coordination sites of the *py*aza chelating ligand.

In contrast to the electroneutral complex **1**, the molecular structures of the cationic complexes **5** and **6** further contain the PF_6^- anion, with the shortest Ir−P distance of 6.4795(11), and 6.1421(13) Å, respectively. The dihedral angles formed by the cyclopentadienyl and 7-azaindole rings equal 24.80(11), 17.04(12), and 23.3(2)° for complexes **1**, **5**, and **6**, respectively. The intraligand dihedral angles between the 7-azaindole moiety and pendant N1-substituent were found to be 17.29(9), 36.67(10), and 31.4(2)° for complexes **1**, **5**, and **6**, respectively. The N(1)−C(8)−X(9)−Ir torsion angles (X = C for **1** and N for **5** and **6**) equal 10.9(5), 12.3(4), and −21.7(7)° for complexes **1**, **5**, and **6**, respectively, while the N(1)−C(7A)−N(7)−Ir torsion angles were −21.9(5), −28.3(5), and 17.3(7)° for complexes **1**, **5**, and **6**, respectively.

The crystal structures of complexes **1**, **5**, and **6** are stabilized by C−H···Cl, C−H···C, and C···C types of noncovalent contacts, while the C−H···F contacts were also found in addition to those mentioned in the crystal structure of the cationic complexes **5** and **6** containing the PF_6^- counterion (Table S3).

Concerning the half-sandwich iridium(III) complexes deposited in the Cambridge Crystallographic Data Centre (CCDC; version 5.39, updated November 2017),[20] only complexes [Ir(η^5-Cp*)(L^1)Cl] (CCDC file 938957)[21] and [Ir(η^5-Cp*)(L^2)Cl] (CCDC file 1033927)[22] can be seen as having compositions similar to the herein reported complexes **1**−**6** (represented by crystallographically characterized complexes **1**, **5**, and **6**) (HL^1 = 3-phenylimidazo[1,2-*a*][1,8]-naphthyridine, HL^2 = 2-(2,3-dihydro-1*H*-inden-1-yl)-pyrimidine). In particular, complexes [Ir(η^5-Cp*)(L^1)Cl] and [Ir(η^5-Cp*)(L^2)Cl] both contain, analogously with complexes

DOI: 10.1021/acs.organomet.8b00415
Organometallics XXXX, XXX, XXX−XXX

Table 2. In Vitro Cytotoxicity ($IC_{50} \pm SD$; μM) of Complexes 1−6 and Cisplatin against Cisplatin-Sensitive Ovarian Carcinoma Cells (A2780) and Cisplatin-Resistant Ovarian Carcinoma Cells (A2780R)[a]

	1	2	3	6	cisplatin
A2780	25.4 ± 2.0	>50.0	20.2 ± 3.2	3.1 ± 0.2	7.1 ± 1.3
A2780R	>50.0	20.3 ± 2.3	>25.0	17.4 ± 1.3	20.6 ± 1.9

[a]MTT assay, 24 h exposure followed by 72 h recovery. Complexes **4** and **5** were inactive up to the highest tested concentration at both cells (IC_{50} > 50.0 μM).

1−**6**, a chelating ligand based on fused six- and five-membered rings with a pendant aromatic substituent, giving together the deprotonated bidentate C,N-donor ligands. Further for the CCDC deposited X-ray structures, the Cp*-containing half-sandwich iridium(III) complexes are numerous in the literature,[3] while crystallographically characterized Cp^{ph} analogues (complex **6** in this work) are quite rare.[6c,23]

In Vitro Cytotoxicity. The in vitro cytotoxicity of complexes **1**−**6** was screened by an MTT assay against two human cancer cell lines: namely, ovarian carcinoma cells naturally sensitive to cisplatin (A2780) and its variant with the acquired resistance to cisplatin (A2780R). The platinum-based drug cisplatin was used as the standard in this study. The obtained in vitro cytotoxicity results are given in Table 2.

Complex **6** had significantly lower IC_{50} values ($p < 0.05$) against the A2780 ovarian carcinoma cells in comparison to cisplatin. However, the obtained results did not show the ability of complex **6** to overcome the acquired resistance of the A2780 cells toward the therapeutic effect of cisplatin, because the calculated resistance factor (RF = IC_{50}(A2780R)/IC_{50}(A2780)) of complex **6** (RF ≈ 5.6) was even higher than for cisplatin (RF ≈ 2.9). In accordance with the literature data reported for similar ionic half-sandwich Ir(III) complexes,[3b,6c,7] the Cp^{ph} complex **6** exceeds the potency of its inactive Cp* analogue **5**. Surprisingly, the same trend was not observed for the group of electroneutral complexes **1**−**4**, where the Cp* complexes exceeded the cytotoxicity of their Cp^{ph} analogues against the A2780 cells. An unusual cytotoxic profile was observed for complex **2**, which showed moderate activity against the resistant A2780R cells, although it was inactive against the A2780 cells.

The representative complexes **1**, **3** and **6**, which were potent against the A2780 cells, were also studied for their toxicity against noncancerous human cells (MRC-5) up to 50.0 μM concentration (Figure 4).

Only complex **1** reached the IC_{50} value (28.3 ± 4.7 μM) within the tested concentration range, indicating low selectivity toward the cancer cells (i.e., A2780) over the noncancerous cells (i.e., MRC-5). Complexes **3** and **6** were markedly less toxic against the MRC-5 cells (IC_{50} > 50.0 μM) in comparison to cisplatin (IC_{50} = 7.2 ± 1.2 μM), suggesting their promising selectivity, especially for the best-performing complex **6**.

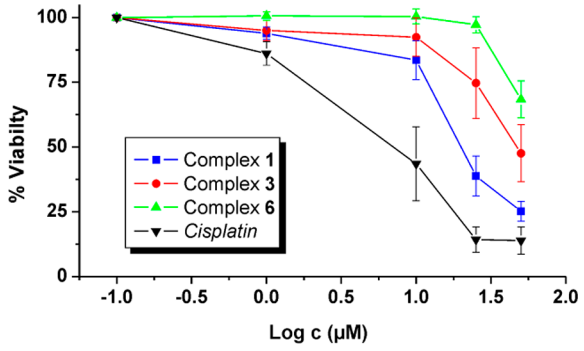

Figure 4. MRC-5 cell viability curves obtained for complexes **1**, **3**, and **6**, given with the reference drug cisplatin.

With respect to the discussed results of cytotoxicity (A2780 and A2780R cells) and toxicity (MRC-5 cells) screening (vide supra), only the leading complex **6** was selected for additional cytotoxicity experiments focusing on its ability to effectively kill cancer cells other than those of ovarian origin. Thus, the cytotoxic effect of complex **6** was tested against a panel of five different human cancer cell lines: namely, prostatic carcinoma cell DU145, lung carcinoma cells A549, colon carcinoma cells HCT116, cervix adenocarcinoma HeLa, and breast adenocarcinoma MCF7. The cytotoxic efficiency of complex **6** in these cell lines was compared to that of clinically used cisplatin. In this experiment, a colorimetric assay based on neutral red uptake was used for in vitro sensitivity testing of cell lines. The MTT assay, commonly used for cytotoxicity testing (and also used in the previous experiment with ovarian cancer cells), requires mitochondrial metabolic activity (measures mitochondria dehydrogenase activity as a marker of cell viability) to convert the colorless tetrazolium to the purple-colored formazan dye. However, a large number of Ir complexes have been shown to interfere with mitochondrial activity[24] so that the metabolization of MTT can reflect an effect of the Ir complexes on the mitochondrial metabolism rather than the viability of cells. Conversely, the neutral red uptake assay is based on the abilities of viable cells to incorporate and bind the dye in lysosomes, so that it is not affected by changes in the mitochondrial metabolism.

Under experimental conditions used in this experiment, complex **6** showed significantly better activity toward colon HCT116 and breast MCF7 cancer cells in comparison to cisplatin (Table 3). However, the sensitivity of other cancer cell lines to complex **6** was either less than (Du-145) or comparable to (HeLa, A549) the sensitivity toward cisplatin. These results indicate that the cytotoxic effect of complex **6** might be selective to certain types of cancer.

In Vitro Cytotoxicity in Spheroid (3D) Culture. Despite the fact that 2D monolayer cell cultures are frequently used for testing of cytotoxic activity of various compounds, including metallodrugs, their utilization is not ideal because 2D cell monolayers represent an environment distinctly different from that in native tumors, in which most of the tissues are 3D with a specific organization and architecture. Hence, three-dimensional (3D) growth of cell cultures is regarded as a more stringent and representative model for in vitro drug screening.[25] Cells growing in 3D cultures possess several in vivo features of tumors such as cell−cell interaction, hypoxia, drug penetration, response, and resistance, and production/deposition of extracellular matrix.[26] Hence, it is now a common opinion that in vitro 3D cultures could fill the gap between conventional 2D in vitro testing and animal models, and the use of 3D cell cultures in drug screening programs is

DOI: 10.1021/acs.organomet.8b00415
Organometallics XXXX, XXX, XXX−XXX

Table 3. In Vitro Cytotoxicity (IC_{50} ± SD; μM) of Complex 6 and Cisplatin in a Panel of Five Human Cell Lines[a]

	HCT116	HeLa	MCF7	DU-145	A549
6	10.4 ± 1.4	10.5 ± 0.7	6.9 ± 0.1	13.0 ± 1.4	9.1 ± 0.7
cisplatin	23.1 ± 1.2	11.9 ± 1.1	21.7 ± 2.1	5.0 ± 0.3	6.0 ± 0.5

[a]The cells were treated for 72 h, and cell viability was evaluated by using an assay based on neutral red. The data represent mean ± SD from at least three independent experiments, each made in quadruplicate.

recommended as support for conventional 2D monolayer studies and before activation of animal protocols.[27] Therefore, in this study, the effect of complex **6** and cisplatin also on 3D cultures of MCF7 cells was tested to provide more relevant data on its antitumor activity.

Under the experimental conditions used in this experiment, the cytotoxicity of complex **6** was ca. 1.5-fold better than that of cisplatin (IC_{50} values determined from two independent experiments were 22.9 ± 2.8 and 35.4 ± 1.0 μM for complex **6** and cisplatin, respectively) (Figure 5). Thus, these results

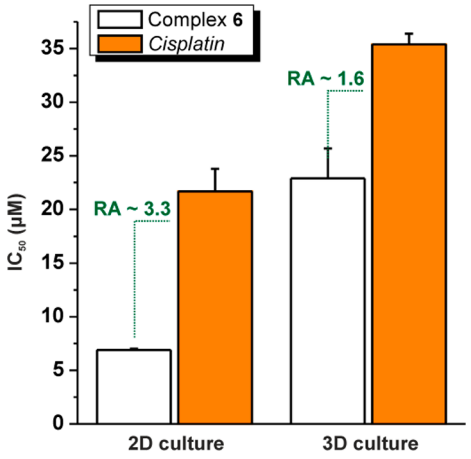

Figure 5. Comparison of cytotoxicities of complex **6** (and cisplatin for comparative purposes) against MCF7 human breast adenocarcinoma cells, as observed at the 2D (adherent cells) and 3D (spheroids) cultures, both studied at a 72 h exposure time. RA stands for relative activity calculated as IC_{50}(cisplatin)/IC_{50}(complex **6**).

confirm the trend found for monolayer MCF7 cells (Table 3); however, the difference between cytotoxicities of complex **6** and cisplatin is less pronounced, which may reflect properties typical for 3D but not for 2D cultures, such as different penetration to the tissue of spheroids.

Hydrophobicity and Cellular Accumulation. Hydrophobicity (lipophilicity) is generally accepted as an important and worthy of study feature of newly developed biologically active compounds, including anticancer transition-metal complexes, mainly because it has been shown as being consistent with their potency.[3b,5d,28] The log *P* values determined for complex **6** by an octanol/water partition (NaCl was added to water to suppress hydrolysis) equaled 0.43 ± 0.01, implying markedly higher lipophilicity than for cisplatin (log *P* = −2.19).[29]

An efficient cellular uptake through the cellular membrane and accumulation in cells represent key factors essential for the biological activity of drugs. In order to assess a possible effect of these processes on the in vitro cytotoxicity of complex **6**, the cellular accumulation of iridium from complex **6** was determined and compared with the cellular accumulation of platinum from the clinically used cisplatin. Cellular levels of Ir or Pt were measured after 24 h exposure of the A2780 cells to complex **6** and cisplatin at their IC_{50} concentrations. The cellular levels of a particular metal were quantified by means of inductively coupled plasma mass spectrometry (ICP-MS) analysis. The accumulation of Ir from lipophilic complex **6** in the A2780 cells after 24 h of incubation (22159 ± 1501 pmol Ir/10^6 cells) was ca. 250-fold greater than the amount of Pt associated with cells treated with hydrophilic cisplatin (86 ± 4 pmol Ir/10^6 cells). Thus, the hydrophobicity (log *P*) and cell accumulation correlate significantly. However, the cytotoxicity of complex **6** in A2780 cells was only ca. 2-fold higher than that of cisplatin (Table 2), so that the cytotoxic activity of complex **6** does not fully reflect elevated uptake and accumulation.

Cell Cycle Analysis. Complex **6** induced the relevant changes of the A2780 cell cycle (Figure 6). In particular, its

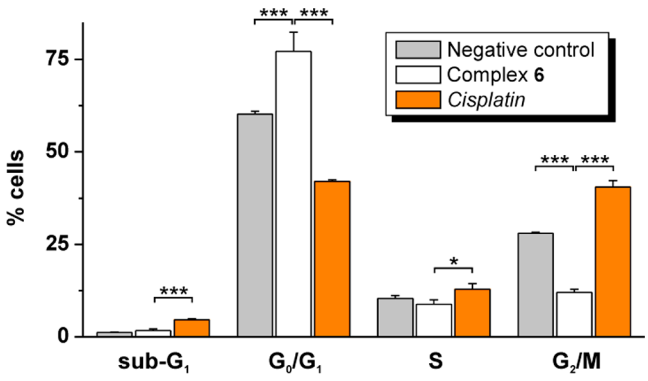

Figure 6. Results (% cells) of the flow cytometry studies (PI/RNase staining) of the A2780 cells treated with complex **6** and with the reference drug cisplatin, given as arithmetic mean from three independent experiments. The significant differences between the obtained results of complex **6** vs the negative control and cisplatin are given as * for $p < 0.05$ and *** for $p < 0.005$.

application to the A2780 cells induced higher cell populations in the G_0/G_1-cell cycle phase (77.2 ± 5.2%) than in the case of the untreated cells (60.0 ± 2.8%) employed as the negative control.

The observed G_0/G_1-cell cycle phase arrest induced by complex **6** was connected with the reduction of the G_2/M-cell cycle phase population of the cells treated by complex **6** (12.0 ± 0.9%) in comparison to that observed for the negative control (23.5 ± 2.1%). The cell cycle perturbation provoked by complex **6** at the used A2780 cells (i.e., G_0/G_1 arrest) was comparable with similar half-sandwich Ir(III) chlorido complexes, such as the apoptosis-inducing complex [Ir(η^5-Cp^{bph})(phen)Cl]PF_6.[3b,30] On the other hand, complex **6** induced different cell cycle perturbation in the used A2780 cells in comparison to the conventional platinum-based drug cisplatin (Figure 6), which is indicative of different mechanisms of action of the studied agents (i.e., **6** vs cisplatin) affecting the cell cycle progression differently.

DOI: 10.1021/acs.organomet.8b00415
Organometallics XXXX, XXX, XXX−XXX

Studies of Hydrolysis and Interactions with Biomolecules in Vitro. For further interaction studies using mass spectrometry, the cationic complex **6** was selected due to its promising biological activities profile (vide supra). At the start of the experiment, in which the hydrolytic properties of complex **6** should have been shown, we obtained a mass spectrum similar to that discussed above (Figure S3), containing the signals (at m/z 425.2, 584.3, and 620.0, corresponding to the $[Ir(Cp^{ph})Cl]^+$, $\{[Ir(Cp^{ph})(pyaza)] - H\}^+$, and $[Ir(Cp^{ph})(pyaza)Cl]^+$, species, respectively) of the intact complex only (Figure S7). After 24 h, the spectrum was enriched by a new peak at m/z 292.7, assignable to the dicationic species $[Ir(Cp^{ph})(pyaza)]^{2+}$, and after 72 h one new peak with low intensity arose at m/z 602.2, corresponding to the $[Ir(Cp^{ph})(pyaza)(OH)]^+$ species.

In contrast to platinum(II) complexes used in anticancer therapy (e.g., cisplatin) having DNA as the dominant molecular target, the molecular targets of the complexes containing iridium are quite variable. Some of these targets are cytosolic or membrane proteins. Due to this fact, interactions with model proteins cytochrome *c* (Cyt *c*) and hen egg white lysozyme (HEWL) were studied in mixtures containing complex **6** on a 72 h time scale. The intensity of these species, corresponding to the intact protein electrostatically bonding one PF_6^- residue (Δ_{mass} = 145 Da), increased to ca. 20% and 30% of the intensity of the intact protein for Cyt *c* and HEWL, respectively after 72 h (see Figure S8).

Another molecular target, very often identified in the context of anticancer activity, is reduced glutathione (GSH) and other antioxidants, depletion of which can upset the metabolic balance in the target cells and induce the process of apoptosis (usually via a mitochondrial pathway).[31] For this reason, the ability of complex **6** to interact with a mixture of two sulfur-containing biomolecules (GSH and L-cysteine (CySH)) applied at normal serum concentrations was investigated by mass spectrometry. As can be seen from Figure 7, the mass spectrum of a mixture containing complex **6** (at 10 μM concentration), GSH (at 6 μM concentration), and CySH (at 290 μM concentration), measured after 72 h of standing at laboratory temperature, contained, in addition to the peaks corresponding to complex **6** (at m/z 425.3, 584.4, and 620.2) and those originating from native and oxidized forms of CySH and GSH (at m/z 122.2, 241.1, and 308.2), also two low-intensity peaks corresponding to the interaction intermediates $[Ir(Cp^{ph})(CyS)]^+$ at m/z 510.2 and $\{[Ir(Cp^{ph})(pyaza)-(CyS)]+H_2O\}^+$ at m/z 722.0. These results confirmed very slow kinetics of the ligand's exchange in the studied complex **6**. The low interaction rate with the biomolecules used may be attributed to the high hydrolytic stability of complex **6**.

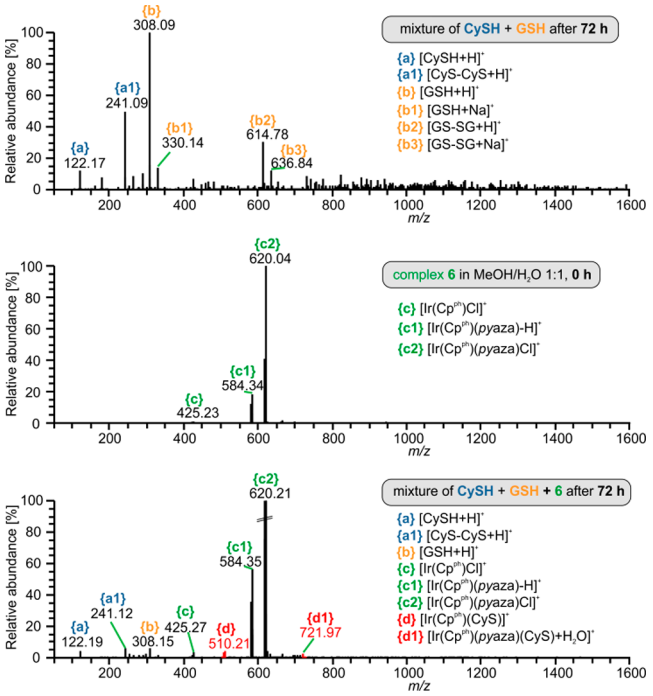

Figure 7. ESI+ mass spectra of a mixture of CySH and GSH after 72 h (top), complex **6** in MeOH/H_2O (1/1, v/v) measured immediately after preparation (middle), and a mixture of complex **6** (at 10 μM concentration), GSH (at 6 μM concentration), and CySH (at 290 μM concentration) measured after 72 h of standing at laboratory temperature (bottom). The specific peak positions and corresponding ionic species are noted.

CONCLUSIONS

Six new half-sandwich iridium(III) complexes were prepared and thoroughly characterized. Complexes contain various N1-derivatives of 7-azaindole (*ph*aza, *th*aza, *py*aza) and various cyclopentadienyl rings (Cp*, Cp^{ph}). The crystallographic studies of complexes **1**, **5**, and **6** proved the 7-azaindole-based ligands to be bidentately coordinated through the N7 atom of the 7-azaindole ring and through either carbon (for phenyl derivative *ph*aza$^-$ of **1**) or nitrogen (for pyridyl derivative *py*aza of **5** and **6**) atom of the pendant N1-substituent. The best-performing complex **6** showed high cytotoxic activity against several of the used human cancer cell lines, high selectivity toward cancer cells over the normal cells, and some relevant differences within the processes connected with its mechanism of action (higher cellular accumulation and different cancer cell cycle perturbation in comparison with conventional cisplatin). Complex **6** was, as the first half-sandwich iridium(III) complex, studied for its cytotoxicity at the spheroid cancer cell culture (MCF7 cells), where it showed higher cytotoxicity in comparison to the platinum-based drug cisplatin.

EXPERIMENTAL SECTION

Materials. $IrCl_3 \cdot nH_2O$ (99%) was purchased from Precious Metals Online, and 1,2,3,4,5-pentamethylcyclopentadiene (95%), 2,3,4,5-tetramethyl-2-cyclopentenone (95%), phenylmagnesium bromide (3.0 M in diethyl ether), 7-azaindole (98%), CuI (≥95%), LiCl (99%), K_2CO_3 (≥99%), bromobenzene (99%), 2-bromopyridine (99%), 2-bromothiophene (98%), NH_4Cl (≥99.5%), $MgSO_4$ (≥99.5%), CH_3COONa (≥99%), NH_4PF_6 (≥98%), KCl (≥99%), L-glutathione reduced (GSH), L-cysteine hydrochloride (CySH·HCl), Cyt *c* from bovine heart, HEWL, and cisplatin (99.9%) were purchased from Sigma-Aldrich and Alfa Aesar Ltd. Solvents of laboratory grade were purchased from Sigma-Aldrich, Fisher-Scientific, and Litolab and used without further purification, except THF that was dried using 4 Å molecular sieves. Deuterated solvents (DMSO-d_6, MeOD-d_4, D_2O) for NMR experiments and MeCN of HPLC grade were purchased from Sigma-Aldrich. Roswell Park Memorial Institute (RPMI-1640) medium, fetal bovine serum, glutamine, penicillin/streptomycin mixture, trypsin, and phosphate-buffered saline (PBS) were purchased from Sigma-Aldrich and Fisher-Scientific.

Synthesis of the Starting Compounds. The starting N1-substituted 7-azaindole derivatives 1-phenyl-7-azaindole (*ph*aza),[11] 1-(pyridin-2-yl)-7-azaindole (*py*aza),[12] and 1-(thiophen-2-yl)-7-azaindole (*th*aza)[13] were prepared using modifications of the previously

DOI: 10.1021/acs.organomet.8b00415
Organometallics XXXX, XXX, XXX−XXX

reported protocols (see the Supporting Information). The iridium(III) dimeric complex $[Ir(\mu\text{-}Cl)(\eta^5\text{-}Cp^*)Cl]_2$ was prepared following the reported procedure,[32] while the reported synthesis of complex $[Ir(\mu\text{-}Cl)(\eta^5\text{-}Cp^{ph})Cl]_2$[23a] was slightly modified (Supporting Information). All of the named starting compounds were synthesized using a Monowave 300 microwave reaction system (Anton Paar).

Synthesis of Complexes 1−6. *$[Ir(\eta^5\text{-}Cp^*)(phaza^-)Cl]$ (1).* The 7-azaindole derivative *ph*aza (0.55 mmol) was dissolved in 2 mL of methanol, and $[Ir(\mu\text{-}Cl)(\eta^5\text{-}Cp^*)Cl]_2$ (0.25 mmol) and CH_3COONa (1.00 mmol) were added. The reaction mixture was stirred at ambient temperature for 30 min. After that, the reaction mixture was filtered and the bright yellow filtrate obtained was concentrated by nitrogen gas until a yellow microcrystalline solid of complex **1** formed. The product was collected by filtration, washed with methanol (1 × 0.5 mL) and diethyl ether (3 × 1 mL), and dried under vacuum (15 min). Yield: 90% (related to the starting Ir(III) dimer). ^{1}H NMR (600 MHz, DMSO-d_6, 300 K): δ 8.54 (d, 1H, J = 4.1 Hz), 8.46 (d, 1H, J = 5.5 Hz), 8.34 (d, 1H, J = 6.9 Hz), 7.70 (d, 1H, J = 8.2 Hz), 7.60 (m, 1H), 7.34 (m, 1H), 7.18 (m, 1H), 7.02 (m, 1H), 6.94 (d, 1H, J = 3.4 Hz), 1.37 (s, 15H) ppm. ^{13}C NMR (600 MHz, DMSO-d_6, 300 K): δ 150.7, 142.1, 136.2, 133.5, 128.5, 126.8, 126.6, 124.9, 124.5, 120.3, 116.7, 104.8, 96.5, 87.8, 8.3 ppm. ^{15}N NMR (600 MHz, DMSO-d_6, 300 K): δ 161.0, 141.9 ppm. ESI+ MS (MeOH; m/z): 521.2 (calcd 521.2 for $[Ir(Cp^*)(phaza^-)]^+$; 100%). Anal. Calcd for $IrC_{23}H_{24}N_2Cl$ (556.12): C, 49.67; H, 4.35; N, 5.04. Found: 49.66; H, 4.48; N, 4.91. Crystals suitable for a single-crystal X-ray analysis were obtained by slow evaporation (ca. 48 h) of a methanolic solution of complex **1** at ambient temperature.

$[Ir(\eta^5\text{-}Cp^{ph})(phaza^-)Cl]$ (2). The synthesis was performed as for complex **1** using the overnight reaction of *ph*aza (0.25 mmol), $[Ir(\mu\text{-}Cl)(\eta^5\text{-}Cp^{ph})Cl]_2$ (0.10 mmol), and sodium acetate (0.40 mmol) in 2 mL of methanol. Yield: 32% (related to the starting Ir(III) dimer). ^{1}H NMR (600 MHz, DMSO-d_6, 300 K): δ 8.41 (d, 1H, J = 3.7 Hz), 8.40 (d, 1H, J = 4.6 Hz), 8.10 (d, 1H, J = 7.3 Hz), 7.53 (m, 1H), 7.41 (d, 1H, J = 8.3 Hz), 7.27 (m, 5H), 7.14 (dd, 1H, J = 8.3, 5.5 Hz), 6.91 (t, 1H, J = 8.3 Hz), 6.82 (d, 1H, J = 3.7 Hz) 6.79 (t, 1H, J = 6.5 Hz), 1.44 (s, 3H), 1.39 (s, 3H), 1.34 (s, 3H), 1.20 (s, 3H) ppm. ^{13}C NMR (600 MHz, DMSO-d_6, 300 K): δ 149.1, 142.9, 136.1, 132.6, 130.7, 129.8, 128.2, 127.1, 124.6, 123.4, 118.6, 114.2, 103.4, 97.0, 86.4, 85.0, 9.7, 8.9 ppm. ^{15}N NMR (600 MHz, DMSO-d_6, 300 K): δ 161.7, 134.3 ppm. ESI+ MS (MeOH; m/z): 583.2 (calcd 583.2 for $[Ir(Cp^{ph})(phaza^-)]^+$; 100%). Anal. Calcd for $IrC_{28}H_{26}N_2Cl$ (618.19): C, 54.40; H, 4.24; N, 4.53. Found: 54.25; H, 4.23; N, 4.47.

$[Ir(\eta^5\text{-}Cp^*)(thaza^-)Cl]$ (3). 1-(Thiophen-2-yl)-7-azaindole (*th*aza; 0.25 mmol) reacted at ambient temperature in methanol (2 mL) for 30 min with $[Ir(\mu\text{-}Cl)(\eta^5\text{-}Cp^*)Cl]_2$ (0.10 mmol). The reaction mixture was filtered, and the yellow filtrate was concentrated using nitrogen gas. The obtained product was collected by filtration, washed with methanol (1 × 0.5 mL) and diethyl ether (3 × 1 mL), and dried under vacuum (15 min). Yield: 80% (related to the starting Ir(III) dimer). ^{1}H NMR (600 MHz, DMSO-d_6, 300 K): ^{1}H NMR (600 MHz, DMSO-d_6, 300 K): δ 8.52 (d, 1H, J = 5.5 Hz), 8.42 (d, 1H, J = 7.3 Hz), 8.10 (d, 1H, J = 3.7 Hz), 7.40 (m, 1H), 7.35 (d, 1H, J = 5.5 Hz), 6.95 (d, 1H, J = 5.5 Hz), 6.92 (d, 1H, J = 3.7 Hz), 1.54 (s, 15H) ppm. ^{13}C NMR (600 MHz, DMSO-d_6, 300 K): δ 150.7, 138.9, 135.7, 133.8, 129.0, 128.5, 123.2, 120.0, 119.1, 111.8, 103.8, 96.0, 8.3 ppm. ^{15}N NMR (600 MHz, DMSO-d_6, 300 K): δ 156.7, 143.6 ppm. ESI+ MS (MeOH; m/z): 527.2 (calcd 527.1 for $[Ir(Cp^*)(thaza^-)]^+$; 100%). Anal. Calcd for $IrC_{21}H_{22}N_2SCl$ (562.15): C, 44.87; H, 3.94; N, 4.98. Found: 44.62; H, 3.76; N, 4.82.

$[Ir(\eta^5\text{-}Cp^{ph})(thaza^-)Cl]$ (4). The synthesis was performed as for **3** using the reaction (3 h) of *th*aza (0.35 mmol) and $[Ir(\mu\text{-}Cl)(\eta^5\text{-}Cp^{ph})Cl]_2$ (0.10 mmol) in 2 mL of methanol. Yield: 62% (related to the starting Ir(III) dimer). ^{1}H NMR (600 MHz, DMSO-d_6, 300 K): δ 8.47 (d, 1H, J = 5.5 Hz), 8.33 (d, 1H, J = 8.3 Hz), 8.16 (d, 1H, J = 3.7 Hz), 7.35 (m, 1H), 7.21 (m, 4H), 6.97 (m, 4H), 2.05 (s, 3H), 1.78 (s, 3H), 1.68 (s, 3H), 1.38 (s, 3H) ppm. ^{13}C NMR (600 MHz, DMSO-d_6, 300 K): δ 151.3, 139.0, 136.4, 134.5, 130−128.8, 123.9, 120.0, 111.6, 105.4, 103.0, 98.6, 93.7, 89.0, 10.2, 9.1 ppm. ^{15}N NMR (600 MHz, DMSO-d_6, 300 K): δ 154.4, 142.0 ppm. ESI+ MS (MeOH; m/z): 589.2 (calcd 589.1 for $[Ir(Cp^{ph})(thaza^-)]^+$; 100%). Anal. Calcd for $IrC_{26}H_{24}N_2SCl$ (624.22): C, 50.03; H, 3.88; N, 4.49. Found: 49.60; H, 3.83; N, 4.12.

$[Ir(\eta^5\text{-}Cp^*)(pyaza)Cl]PF_6$ (5). The starting iridium(III) dimer $[Ir(\mu\text{-}Cl)(\eta^5\text{-}Cp^*)Cl]_2$ (0.10 mmol) was poured into a solution of *py*aza (0.25 mmol) in 2 mL of methanol. The yellow reaction mixture was filtered after 30 min of stirring at ambient temperature, and an excess of NH_4PF_6 (0.50 mmol) was added. The mixture was stirred for 10 min and then concentrated by nitrogen gas until a yellow microcrystalline product formed. The product was collected by filtration, washed with methanol (1 × 0.5 mL) and diethyl ether (3 × 1 mL), and dried under vacuum (15 min). Yield: 85% (related to the starting Ir(III) dimer). ^{1}H NMR (600 MHz, DMSO-d_6, 300 K): δ 8.72 (d, 1H, J = 5.5 Hz), 8.57 (d, 1H, J = 4.6 Hz), 8.47 (d, 1H, J = 5.5 Hz), 8.38 (d, 1H, J = 8.3 Hz), 8.28 (m, 1H), 8.12 (d, 1H, J = 8.3 Hz), 7.59 (m, 1H), 7.54 (m, 1H), 7.18 (d, 1H, J = 4.6 Hz), 1.32 (s, 15H) ppm. ^{13}C NMR (600 MHz, DMSO-d_6, 300 K): δ 154.8, 148.2, 147.2, 144.0, 142.4, 133.6, 128.6, 124.4, 123.6, 122.2, 115.5, 108.2, 88.5, 7.9 ppm. ^{15}N NMR (600 MHz, DMSO-d_6, 300 K): δ 188.4, 173.0, 154.3 ppm. ESI+ MS (MeOH; m/z): 558.0 (calcd 558.1 for $[Ir(Cp^*)(pyaza)Cl]^+$; 50%), 522.2 (calcd 522.2 for $\{[Ir(Cp^*)(pyaza)] - H\}^+$; 100%). Anal. Calcd for $IrC_{22}H_{24}N_3ClPF_6$ (703.08): C, 37.58; H, 3.44; N, 5.98. Found: 37.42; H, 3.36; N, 6.07. Crystals of complex **2** suitable for a single-crystal X-ray analysis were obtained by slow evaporation (ca. 24 h) of its methanolic solution at ambient temperature.

$[Ir(\eta^5\text{-}Cp^{ph})(pyaza)Cl]PF_6$ (6). The synthesis was performed as for complex **5** using the reaction of *py*aza (0.35 mmol), $[Ir(\mu\text{-}Cl)(\eta^5\text{-}Cp^{ph})Cl]_2$ (0.10 mmol), and NH_4PF_6 (0.50 mmol). Yield: 80% (related to the starting Ir(III) dimer). ^{1}H NMR (600 MHz, DMSO-d_6, 300 K): δ 8.72 (d, 1H, J = 5.5 Hz), 8.59 (d, 1H, J = 4.6 Hz), 8.39 (d, 1H, J = 5.5 Hz), 8.36 (d, 1H, J = 8.3 Hz), 8.27 (t, 1H, J = 7.3 Hz), 8.12 (d, 1H, J = 8.3 Hz), 7.46 (m, 7H), 7.19 (d, 1H, J = 3.7 Hz), 1.47 (s, 3H), 1.42 (s, 3H), 1.39 (s, 3H), 1.23 (s, 3H) ppm. ^{13}C NMR (600 MHz, DMSO-d_6, 300 K): δ 154.8, 148.2, 147.2, 144.0, 142.4, 133.6, 129.4−128.6, 124.4, 123.6, 122.2, 115.5, 108.2, 97.1, 96.6, 87.1, 81.3, 9.1, 8.1 ppm. ^{15}N NMR (600 MHz, DMSO-d_6, 300 K): δ 185.8, 169.7, 153.3 ppm. ESI+ MS (MeOH; m/z): 620.0 (calcd 620.1 for $[Ir(Cp^{ph})(pyaza)Cl]^+$; 85%), 584.2 (calcd 584.2 for $\{[Ir(Cp^{ph})(pyaza)] - H\}^+$; 100%). Anal. Calcd for $IrC_{27}H_{26}N_3ClPF_6$ (765.15): C, 42.38; H, 3.42; N, 5.49. Found: 42.03; H, 3.05; N, 5.11.

General Methods. Elemental analyses were carried out using a Flash 2000 CHNS Elemental Analyzer (Thermo Scientific). Electrospray ionization mass spectrometry (ESI-MS) was performed with an LCQ Fleet ion trap spectrometer (Thermo Scientific; QualBrowser software, version 2.0.7) in positive ionization mode (ESI+) on methanolic solutions of the studied complexes. ^{1}H, ^{13}C, ^{1}H−^{1}H gs-COSY, ^{1}H−^{13}C gs-HMQC, ^{1}H−^{13}C gs-HMBC and ^{1}H−^{15}N gs-HMBC spectra were recorded using a JEOL JNM-ECA 600II device on DMSO-d_6 solutions of the starting compounds and the studied complexes at 300 K (gs = gradient selected, COSY = correlation spectroscopy, HMQC = heteronuclear multiple quantum coherence, HMBC = heteronuclear multiple bond coherence). ^{1}H and ^{13}C NMR spectra were calibrated against the residual signal of the solvent found at 2.50 ppm (^{1}H) and 39.5 ppm (^{13}C),[33] while ^{1}H−^{15}N gs-HMBC spectra were calibrated externally against the signals of DMF found at 8.03 ppm (^{1}H) and 104.7 ppm (^{15}N). The splitting of proton resonances in the reported ^{1}H spectra is defined as s = singlet, d = doublet, t = triplet, br = broad band, m = multiplet. Coordination shifts ($\Delta\delta$; ppm) were calculated as $\delta_{complex} - \delta_{ligand}$. Infrared spectra (400−4000 cm^{-1}, ATR technique) were acquired with a Nexus 670 FT-IR instrument (Thermo Nicolet). Reversed-phase high-performance liquid chromatography (RP-HPLC) coupled to positive electrospray ionization mode mass spectrometry (ESI+ MS) was carried out using a UHPLC-MS instrument (Dionex/Thermo Fisher Scientific) equipped with an ReproSil-Pur Basic C18 column (5 μm pore size, 200 × 4.6 mm), with MeCN used as the mobile phase (the detection wavelength was 254 nm).

X-ray Crystallography. The X-ray diffraction data of complexes **1**, **5**, and **6** were collected with a Bruker D8 QUEST diffractometer

DOI: 10.1021/acs.organomet.8b00415
Organometallics XXXX, XXX, XXX−XXX

(Mo Kα radiation) equipped with a PHOTON 100 CMOS detector. The obtained data were processed and reduced by the APEX3 software package,[34] and the molecular structures of complexes **1**, **5**, and **6** were solved by direct methods (SHELXS) and refined by a full-matrix least-squares procedure (SHELXL).[35] Hydrogen atoms of all the structures were found in the difference Fourier maps and refined using a riding model with C−H = 0.95 Å for $CH_{aromatic}$ and 0.98 Å for CH_3, and with $U_{iso}(H) = 1.2\ U_{eq}(CH)$ and $1.5\ U_{eq}(CH_3)$. The F2, F4, and F5 atoms of the hexafluorophosphate anion in complex **5** were refined as disordered over two positions with a 0.53/0.47 combination of occupancy factors. X-ray crystallographic data for complexes **1**, **5**, and **6** have been deposited with the Cambridge Crystallographic Data Centre under the CCDC numbers 1844497, 1844498, and 1844499, respectively. The crystal data and structure refinement details are given in Table S2. The graphics were drawn and additional structural calculations were performed by DIAMOND[36] and Mercury[37] software.

Cell Culture. The human ovarian carcinoma (A2780), cisplatin-resistant ovarian carcinoma (A2780R), and human normal lung fibroblast cell lines (MRC-5) (supplied by European Collection of Cell Cultures, ECACC) were cultured, according to the ECACC instructions, in the RPMI-1640 medium supplemented with 10% of fetal calf serum, 1% of 2 mM glutamine, and 1% penicillin/streptomycin. Human prostatic carcinoma DU-145, human lung carcinoma cells A549, human colon carcinoma cells HCT116, human cervix adenocarcinoma HeLa, and human breast adenocarcinoma MCF7 were cultured in DMEM high glucose supplemented with heat-inactivated FBS (10%) and antibiotics (streptomycin 100 μg mL^{-1}, penicillin 100 U mL^{-1}). All cell lines were grown as adherent monolayers at 37 °C and 5% CO_2 under a humidified atmosphere.

In Vitro Cytotoxicity Testing. An appropriate amount of complexes **1**−**6**, cisplatin, or oxaliplatin was dissolved in 500 μL of DMF to give stock solutions of 50 mM concentration. The stock solutions were diluted by RPMI-1640 medium to concentrations of 0.01−25.0 μM (for **3**) and 0.01−50.0 μM (for **1**, **2**, **4**−**6**, and cisplatin).

The A2780 and A2780R cells were seeded to 96-well culture plates, preincubated in drug-free media at 37 °C for 24 h, and treated with various concentrations of complexes **1**−**6** and standards. After 24 h of drug exposure, the supernatants were removed and the cells were washed with drug-free PBS followed by 72 h recovery in drug-free medium at 37 °C. In parallel, the cells were also treated with 0.1% DMF and 1% Triton X-100 to assess the minimal and maximal cell damage, respectively. The MTT assay (MTT = 3-(4,5-dimethylthiazol-2-yl)-2,5-diphenyltetrazolium bromide) was used to determine the cell viability. The concentration of the formed dye was evaluated spectrophotometrically at 540 nm (TECAN, Schoeller Instruments LLC). The same experiments were performed at the MRC-5 cells, but only for complexes **1**, **3**, and **6** (and cisplatin for comparative purposes).

The DU-145, A549, HCT116, HeLa, and MCF7 cells were seeded in 96-well tissue culture plates at a density of 10000 cells/well. After overnight incubation, the cells were treated with the investigated compounds and kept for 72 h under cultivation conditions. Stock solutions of complex **6** and cisplatin were always freshly prepared in DMF before use, and concentrations of Ir and Pt in cultivation media were always checked by atomic absorption spectrometry (Varian AA240Z Zeeman atomic absorption spectrometer equipped with a GTA 120 graphite tube atomizer). After the treatment period, 20 μL of a 0.33% solution of neutral red in culture medium was added to each well with adherent cells and the plate was incubated at 37 °C under a humidified 5% CO_2 atmosphere for 2 h. Afterward, the dye was carefully removed and the cells were quickly rinsed with PBS. The incorporated dye was then solubilized in 200 μL of 1% acetic acid in 50% ethanol, plates were allowed to stand for 10 min at room temperature, and the absorbance was measured at 540 nm (absorbance reader Synergy Mx, Biotek, USA).

The data from the cancer cells were acquired from three independent experiments (conducted in triplicate) using cells from different passages. The data were expressed as the percentage of viability, and the resulting IC_{50} values (μM), calculated from viability curves, are given as arithmetic mean ± SD. The significance of the differences between the obtained results ($p < 0.05$, $p < 0.01$, and $p < 0.005$ considered to be significant) was assessed by an ANOVA analysis (QC Expert 3.2, Statistical software, TriloByte Ltd.).

Cytotoxicity Testing in Spheroid Culture (3D Culture) of MCF7 Cells. The human Caucasian breast adenocarcinoma cells (derived from the pleural effusion MCF7 cells) were transferred as single cells to 96-well ultralow attachment plates (ULA; Corning, NY, USA), cultivated for 144 h in DMEM medium supplemented with 2% B27 (Thermo Fisher Scientific Inc., MA, USA), 20 ng mL^{-1} epidermal growth factor (EGF; Sigma-Aldrich, Darmstadt, Germany), and 0.15% (w/v) human serum albumin (HSA; Sigma-Aldrich, Darmstadt, Germany). Then, the cells were treated with various concentrations of the investigated compounds and incubated for another 72 h. After the treatment period, the wells were filled with an equal amount of CellTiter-Glo 3D Reagent (100 μL) and the plates were vigorously mixed for 5 min followed by 25 min of incubation at room temperature. Cell viability was evaluated by measuring the luminescence using an Infinite 200 PRO NanoQuant luminescence reader (Tecan). IC_{50} values were calculated from curves constructed by plotting cell survival (%) versus drug concentration (μM). All experiments were done in triplicate. The reading values were converted to the percentage of control (% cell survival).

Hydrophobicity Studies (log *P*). Octanol-saturated water (OSW) and water-saturated octanol (WSO) were prepared from octanol and a 0.2 M water solution of NaCl by overnight shaking (Vibramax 100, Heidolph Instruments). The stock solution was prepared by dissolving 3 μmol of complex **6** in 20 mL of OSW (ultrasonicated for 30 min). The mixture was centrifuged (5 min, 11000 rpm), and the supernatant was collected. A 5 mL portion of this solution was added to 5 mL of WSO and shaken for 2 h at ambient temperature. After that, the mixture was centrifuged, the aqueous layer was separated carefully, and the Ir concentration was determined by ICP-MS (the obtained value was corrected for adsorption effects). The equation $\log P = \log([Ir]WSO/[Ir]OSW_a)$ was used for the partition coefficient calculation; $[Ir]OSW_b$ and $[Ir]OSW_a$ stand for the Ir concentration before and after partition, respectively, and $[Ir]WSO = [Ir]OSW_b - [Ir]OSW_a$. The experiment was conducted in triplicate, and the results are presented as arithmetic mean ± SD.

Cellular Accumulation. The A2780 cells were seeded in six-well culture plates (1×10^6 cells per well) and cultured for 24 h at 37 °C and 5% CO_2 humidified atmosphere in complete growth RPMI-1640 medium. Subsequently, the medium was removed, the cells were washed with PBS, and fresh medium was added. The cells were treated with complex **6** and cisplatin at their IC_{50} concentrations for 24 h. Stock solutions of metal complexes were always freshly prepared in DMF and diluted to the cultivation media so that the final concentration of DMF in cell culture medium did not exceed 0.2% (v/v). After an incubation period, cells were harvested by trypsinization, thoroughly washed with PBS, and collected by centrifugation. Cell pellets were digested in 500 μL of nitric acid (3 min, 150 °C) using a Monowave 300 instrument to give a fully homogenized solution, which was diluted with 4.5 mL of water, and the final iridium or platinum content was determined by ICP-MS (Agilent 7700x, Agilent, Japan). The obtained values were corrected for adsorption effects. The experiments were conducted in triplicate, and the results are presented as arithmetic mean ± SD.

Cell Cycle Analysis. The A2780 cells (1.0×10^6 per well) were preincubated in a six-well plate for 24 h as described above. Complex **6** (cisplatin was involved in the study for comparative purposes) was added at its IC_{50} concentration (determined at the used cell line). After 24 h, the drug-containing medium was removed and the attached cells were harvested using trypsin/EDTA in PBS. The cells were washed twice with PBS and fixed in 70% ethanol. Cells were resuspended in PBS, and DNA staining was achieved by a solution of propidium iodide (PI) supplemented with RNaseA (30 min, 25 °C, in the dark). After that, the cells were resuspended and DNA content was measured using flow cytometry (CytoFlex, Beckman Coulter),

DOI: 10.1021/acs.organomet.8b00415
Organometallics XXXX, XXX, XXX−XXX

detecting the emission of DNA-bound PI (maximum at 617 nm) after excitation at 535 nm. The data were analyzed using CytExpert software (Beckman Coulter).

Studies of Hydrolysis and Interactions with Biomolecules. The ESI+ MS studies of interactions of complex **6** with sulfur-containing GSH and CySH were performed as follows: complex **6** was dissolved in MeOH (500 μL, 10 μM final concentration), and 500 μL of the mixture of normal serum concentrations[38] of GSH (6 μM final concentration) and CySH (290 μM final concentration) in H_2O was added. The obtained solutions were mixed properly, and the ESI+ mass spectra were recorded immediately after preparation and after 24 h and 72 h of standing at laboratory temperature. The methanol solution of complex **6** and solution of complex **6** in an MeOH/H_2O mixture (1/1, v/v) were used as reference solutions in this experiment. The water-containing solution should provide a clue about the hydrolytic behavior of complex **6**.

Additionally, the interactions of complex **6** with the model proteins HEWL and Cyt *c* were studied by means of ESI+ mass spectrometry. The samples contained mixtures of complex **6** (at the 10 μM final concentration) with HEWL or Cyt *c* (at ca. 3 μM final concentration) in an MeOH/H_2O mixture (1/1, v/v). The ESI+ mass spectra were recorded immediately after preparation and then after 24 and 72 h of standing at laboratory temperature. The specific experimental conditions were as follows: the sample solutions were introduced into the mass spectrometer by an HPLC (Dionex UltiMate 3000; Thermo Scientific; Waltham, MA, USA) autosampler in 50 μL spikes into a continual flow of methanol (0.2 mL/min flow rate), and the ionization source was set to 5.3 kV spray voltage and 110 V and 275 °C capillary voltage and temperature. The ESI+ MS spectra were acquired in the range of m/z 50−2000, and the raw spectra of proteins and mixtures thereof were deconvoluted using Promass for Xcalibur ver. 3.0, rev. 10 software (Novatia LLC, Newtown, PA, USA) producing the neutral mass spectra, representing the interacting intermediates.

■ ASSOCIATED CONTENT

Supporting Information

The Supporting Information is available free of charge on the ACS Publications website at DOI: 10.1021/acs.organomet.8b00415.

Details of synthesis and characterization of *ph*aza, *py*aza, *th*aza, and $[Ir(\mu\text{-}Cl)(\eta^5\text{-}Cp^{ph})Cl]_2$, FT-IR spectral data for complexes **1**−**6**, structural formulas of the starting compounds\, ESI+ mass spectra and ^1H NMR spectra, results of ESI-MS studies of hydrolysis and interaction with model protein cytochrome *c*, results of HPLC-MS analysis, crystal data and structure refinement details, and parameters of the noncovalent contacts (PDF)

Accession Codes

CCDC 1844497−1844499 contain the supplementary crystallographic data for this paper. These data can be obtained free of charge via www.ccdc.cam.ac.uk/data_request/cif, or by emailing data_request@ccdc.cam.ac.uk, or by contacting The Cambridge Crystallographic Data Centre, 12 Union Road, Cambridge CB2 1EZ, UK; fax: +44 1223 336033.

■ AUTHOR INFORMATION

Corresponding Author

*E-mail for P.S.: pavel.starha@upol.cz.

ORCID

Pavel Štarha: 0000-0003-0422-045X

Zdeněk Trávníček: 0000-0002-5890-7874

Jana Kašpárková: 0000-0002-5279-5381

Notes

The authors declare no competing financial interest.

■ ACKNOWLEDGMENTS

The authors gratefully thank the Ministry of Education, Youth and Sports of the Czech Republic (projects LO1305 and CZ.1.05/2.1.00/19.0377) and the Czech Science Foundation (GAČR 17-08512Y) for financial support. The authors also thank Ms. Eva Máčalová for her help with syntheses of complexes **1**−**6**, Ms. Kateřina Kubešová for performing part of the cell-based studies, Dr. Peter Antal for recording the NMR spectra, Dr. Bohuslav Drahoš for recording the ESI-MS and HPLC data, Mrs. Pavla Richterová for performing elemental analysis, and Dr. Alena Klanicová for recording the FTIR spectra. The work of H.C. and J.K. was supported by the student project of the Palacky University in Olomouc (IGA_PrF_2018_022).

■ REFERENCES

(1) Kelland, L. The resurgence of platinum-based cancer chemotherapy. *Nat. Rev. Cancer* **2007**, *7*, 573−584.

(2) Gasser, G.; Ott, I.; Metzler-Nolte, N. Organometallic anticancer compounds. *J. Med. Chem.* **2011**, *54*, 3−25.

(3) (a) Leung, C. H.; Zhong, H. J.; Chan, D. S. H.; Ma, D. L. Bioactive iridium and rhodium complexes as therapeutic agents. *Coord. Chem. Rev.* **2013**, *257*, 1764−1776. (b) Liu, Z.; Sadler, P. J. Organoiridium complexes: Anticancer agents and catalysts. *Acc. Chem. Res.* **2014**, *47*, 1174−1185. (c) Li, J. J.; Tian, M.; Tian, Z.; Zhang, S.; Yan, C.; Shao, C.; Liu, Z. Half-sandwich iridium(III) and ruthenium(II) complexes containing P̂P-chelating ligands: A new class of potent anticancer agents with unusual redox features. *Inorg. Chem.* **2018**, *57*, 1705−1716. (d) Wang, C.; Liu, J.; Tian, Z.; Tian, M.; Tian, L.; Zhao, W.; Liu, Z. *Dalton Trans.* **2017**, *46*, 6870−6883. (e) Hearn, J. M.; Hughes, G. M.; Romero-Canelón, I.; Munro, A. F.; Rubio-Ruiz, B.; Liu, Z.; Carragher, N. O.; Sadler, P. J. Pharmaco-genomic investigations of organo-iridium anticancer complexes reveal novel mechanism of action. *Metallomics* **2018**, *10*, 93−107. (f) Petrini, A.; Pettinari, R.; Marchetti, F.; Pettinari, C.; Therrien, B.; Galindo, A.; Scopelliti, R.; Riedel, T.; Dyson, P. J. Cytotoxic half-sandwich Rh(III) and Ir(III) β-diketonates. *Inorg. Chem.* **2017**, *56*, 13600−13612. (g) Zimbron, J. M.; Passador, K.; Gatin-Fraudet, B.; Bachelet, C. M.; Plazuk, D.; Chamoreau, L. M.; Botuha, C.; Thorimbert, S.; Salmain, M. Synthesis, photophysical properties, and living cell imaging of theranostic half-sandwich iridium−4,4-difluoro-4-bora-3*a*,4*a*-diaza-*s*-indacene (BODIPY) Dyads. *Organometallics* **2017**, *36*, 3435−3442.

(4) Romero-Canelón, I.; Sadler, P. J. Next-generation metal anticancer complexes: Multitargeting via redox modulation. *Inorg. Chem.* **2013**, *52*, 12276−12291.

(5) (a) Mukhopadhyay, S.; Gupta, R. K.; Paitandi, R. P.; Rana, N. K.; Sharma, G.; Koch, B.; Rana, L. K.; Hundal, M. S.; Pandey, D. S. Synthesis, structure, DNA/protein binding, and anticancer activity of some half-sandwich cyclometalated Rh(III) and Ir(III) complexes. *Organometallics* **2015**, *34*, 4491−4506. (b) Yellol, J.; Pérez, S. A.; Buceta, A.; Yellol, G.; Donaire, A.; Szumlas, P.; Bednarski, P. J.; Makhloufi, G.; Janiak, C.; Espinosa, A.; Ruiz, J. Novel C,N-cyclometalated benzimidazole ruthenium(II) and iridium(III) complexes as antitumor and antiangiogenic agents: A structure−activity relationship study. *J. Med. Chem.* **2015**, *58*, 7310−7327. (c) Lord, R. M.; Hebden, A. J.; Pask, C. M.; Henderson, I. R.; Allison, S. J.; Shepherd, S. L.; Phillips, R. M.; McGowan, P. C. Hypoxia-sensitive metal β-ketoiminato complexes showing induced single-strand DNA breaks and cancer cell death by apoptosis. *J. Med. Chem.* **2015**, *58*, 4940−4953. (d) Millett, A. J.; Habtemariam, A.; Romero-Canelón, I.; Clarkson, G. J.; Sadler, P. J. Contrasting anticancer activity of half-sandwich iridium(III) complexes bearing functionally diverse 2-phenylpyridine ligands. *Organometallics* **2015**, *34*, 2683−2694.

(6) (a) Liu, Z.; Salassa, L.; Habtemariam, A.; Pizarro, A. M.; Clarkson, G. J.; Sadler, P. J. Contrasting reactivity and cancer cell cytotoxicity of isoelectronic organometallic iridium(III) complexes. *Inorg. Chem.* **2011**, *50*, 5777−5783. (b) Liu, Z.; Habtemariam, A.;

DOI: 10.1021/acs.organomet.8b00415
Organometallics XXXX, XXX, XXX−XXX

Pizarro, A.; Clarkson, G. J.; Sadler, P. J. Organometallic iridium(III) cyclopentadienyl anticancer complexes containing C,N-chelating ligands. *Organometallics* **2011**, *30*, 4702−4710. (c) Liu, Z.; Habtemariam, A.; Pizarro, A. M.; Fletcher, S. A.; Kisova, A.; Vrana, O.; Salassa, L.; Bruijnincx, P. C. A.; Clarkson, G. J.; Brabec, V.; Sadler, P. J. Organometallic half-sandwich iridium anticancer complexes. *J. Med. Chem.* **2011**, *54*, 3011−3026.

(7) Štarha, P.; Habtemariam, A.; Romero-Canelón, I.; Clarkson, G. J.; Sadler, P. J. Hydrogensulfide adducts of organo-iridium anticancer complexes. *Inorg. Chem.* **2016**, *55*, 2324−2331.

(8) (a) Farmer, L. J.; Ledeboer, M. W.; Hoock, T.; Arnost, M. J.; Bethiel, R. S.; Bennani, Y. L.; Black, J. J.; Brummel, C. L.; Chakilam, A.; Dorsch, W. A.; Fan, B.; Cochran, J. E.; Halas, S.; Harrington, E. M.; Hogan, J. K.; Howe, D.; Huang, H.; Jacobs, D. H.; Laitinen, L. M.; Liao, S.; Mahajan, S.; Marone, V.; Martinez-Botella, G.; McCarthy, P.; Messersmith, D.; Namchuk, M.; Oh, L.; Penney, M. S.; Pierce, A. C.; Raybuck, S. A.; Rugg, A.; Salituro, F. G.; Saxena, K.; Shannon, D.; Shlyakter, D.; Swenson, L.; Tian, S. K.; Town, C.; Wang, J.; Wang, T.; Wannamaker, M. W.; Winquist, R. J.; Zuccola, H. J. Discovery of VX-509 (Decernotinib): A potent and selective Janus Kinase 3 inhibitor for the treatment of autoimmune diseases. *J. Med. Chem.* **2015**, *58*, 7195−7216. (b) Esteve, C.; González, J.; Gual, S.; Vidal, L.; Alzina, S.; Sentellas, S.; Jover, I.; Horrillo, R.; De Alba, J.; Miralpeix, M.; Tarrasón, G.; Vidal, B. Discovery of 7-azaindole derivatives as potent Orai inhibitors showing efficacy in a preclinical model of asthma. *Bioorg. Med. Chem. Lett.* **2015**, *25*, 1217−1222.

(9) (a) Štarha, P.; Trávníček, Z.; Popa, A.; Popa, I.; Muchová, T.; Brabec, V. How to modify 7-azaindole to form cytotoxic Pt(II) complexes: Highly in vitro anticancer effective cisplatin derivatives involving halogeno-substituted 7-azaindole. *J. Inorg. Biochem.* **2012**, *115*, 57−63. (b) Štarha, P.; Vančo, J.; Trávníček, Z.; Hošek, J.; Klusáková, J.; Dvořák, Z. Platinum(II) iodido complexes of 7-azaindoles with significant antiproliferative effects: an old story revisited with unexpected outcomes. *PLoS One* **2016**, *11*, e0165062. (c) Štarha, P.; Trávníček, Z.; Pazderová, L.; Dvořák, Z. Platinum(II) carboxylato complexes containing 7-azaindoles as N-donor carrier ligands showed cytotoxicity against cancer cell lines. *J. Inorg. Biochem.* **2016**, *162*, 109−116. (d) Pracharova, J.; Saltarella, T.; Radosova Muchova, T.; Scintilla, S.; Novohradsky, V.; Novakova, O.; Intini, F. P.; Pacifico, C.; Natile, G.; Ilik, P.; Brabec, V.; Kasparkova, J. Novel antitumor cisplatin and transplatin derivatives containing 1-methyl-7-azaindole: synthesis, characterization, and cellular responses. *J. Med. Chem.* **2015**, *58*, 847−859. (e) Zamora, A.; Rodríguez, V.; Cutillas, N.; Yellol, G. S.; Espinosa, A.; Samper, K. G.; Capdevila, M.; Palacios, Ó.; Ruiz, J. New steroidal 7-azaindole platinum(II) antitumor complexes. *J. Inorg. Biochem.* **2013**, *128*, 48−56. (f) Štarha, P.; Trávníček, Z.; Drahoš, B.; Dvořák, Z. In vitro antitumor active gold(I) triphenylphosphane complexes containing 7-azaindoles. *Int. J. Mol. Sci.* **2016**, *17*, 2084.

(10) Štarha, P.; Hanousková, L.; Trávníček, Z. Organometallic half-sandwich dichloridoruthenium(II) complexes with 7-azaindoles: synthesis, characterization and elucidation of their anticancer inactivity against A2780 cell line. *PLoS One* **2015**, *10*, e0143871.

(11) Hong, C. S.; Seo, J. Y.; Yum, E. K. N-Arylation of azaindoles in LiCl-mediated catalytic CuI reactions. *Tetrahedron Lett.* **2007**, *48*, 4831−4833.

(12) Wu, Q.; Lavigne, J. A.; Tao, Y.; D'Iorio, M.; Wang, S. Blue-luminescent/electroluminescent Zn(II) compounds of 7-azaindole and *N*-(2-pyridyl)-7-azaindole: $Zn(7\text{-azaindole})_2(CH_3COO)_2$, $Zn(NPA)(CH_3COO)_2$, and $Zn(NPA)((S)\text{-}(+)\text{-}CH_3CH_2CH(CH_3)COO)_2$ (NPA = *N*-(2-pyridyl)-7-azaindole). *Inorg. Chem.* **2000**, *39*, 5248−5254.

(13) Hong, J. S.; Shim, H. S.; Kim, T. J.; Kang, Y. (N-7-Azaindolyl)oligothiophenes: synthesis, characterization, and photophysical properties. *Tetrahedron* **2007**, *63*, 8761−8769.

(14) Zhao, S. B.; McCormick, T.; Wang, S. Ambient-temperature metal-to-ligand charge-transfer phosphorescence facilitated by triarylboron: Bnpa and its metal complexes. *Inorg. Chem.* **2007**, *46*, 10965−10967.

(15) Zhao, S. B.; Wang, R. Y.; Wang, S. Intramolecular C−H activation directed self-assembly of an organoplatinum(II) molecular square. *J. Am. Chem. Soc.* **2007**, *129*, 3092−3093.

(16) Moore, S. A.; Davies, D. L.; Karim, M. M.; Nagle, J. K.; Wolf, M. O.; Patrick, B. O. Photophysical behaviour of cyclometalated iridium(III) complexes with phosphino(terthiophene) ligands. *Dalton Trans.* **2013**, *42*, 12354−12363.

(17) Bleeke, J. R.; Putprasert, P.; Thananatthanachon, T.; Rath, N. P. Synthesis and characterization of fused-ring iridapyrroles. *Organometallics* **2008**, *27*, 5744−5747.

(18) Bencze, E.; Lokshin, B. V.; Mink, J.; Herrmann, W. A.; Kühn, F. E. Vibrational spectra and structure of the cyclopentadienyl-anion (Cp^-), the pentamethylcyclopentadienyl-anion (Cp^{*-}) and of alkali metal cyclopentadienyls CpM and Cp*M (M = Li, Na, K). *J. Organomet. Chem.* **2001**, *627*, 55−66.

(19) Govindaswamy, P.; Mozharivskyj, Y. A.; Kollipara, M. R. Syntheses, spectral and structural studies of Schiff base complexes of η^5-pentamethylcyclopentadienyl rhodium and iridium. *Polyhedron* **2005**, *24*, 1710−1716.

(20) Allen, F. H. The Cambridge Structural Database: a quarter of a million crystal structures and rising. *Acta Crystallogr., Sect. B: Struct. Sci.* **2002**, *58*, 380−388.

(21) Daw, P.; Ghatak, T.; Doucet, H.; Bera, J. K. Cyclometalations on the imidazo[1,2-*a*][1,8]naphthyridine framework. *Organometallics* **2013**, *32*, 4306−4313.

(22) Wu, Y.; Yang, Y.; Zhou, B.; Li, Y. Iridium(III)-catalyzed C-7 selective C−H alkynylation of indolines at room temperature. *J. Org. Chem.* **2015**, *80*, 1946−1951.

(23) (a) Morris, D. M.; McGeagh, M.; De Peña, D.; Merola, J. S. Extending the range of pentasubstituted cyclopentadienyl compounds: The synthesis of a series of tetramethyl(alkyl or aryl)-cyclopentadienes (Cp^{*R}), their iridium complexes and their catalytic activity for asymmetric transfer hydrogenation. *Polyhedron* **2014**, *84*, 120−135. (b) Liu, Z.; Romero-Canelón, I.; Habtemariam, A.; Clarkson, G. J.; Sadler, P. J. Potent half-sandwich iridium(III) anticancer complexes containing C^N-chelated and pyridine ligands. *Organometallics* **2014**, *33*, 5324−5333.

(24) (a) Li, Y.; Liu, B.; Lu, X. R.; Li, M. F.; Ji, L. N.; Mao, Z. W. Cyclometalated iridium(III) N-heterocyclic carbene complexes as potential mitochondrial anticancer and photodynamic agents. *Dalton Trans.* **2017**, *46*, 11363−11371. (b) Li, Y.; Tan, C. P.; Zhang, W.; He, L.; Ji, L. N.; Mao, Z. W. Phosphorescent iridium(III)-bis-*N*-heterocyclic carbene complexes as mitochondria-targeted theranostic and photodynamic anticancer agents. *Biomaterials* **2015**, *39*, 95−104. (c) Hearn, J. M.; Romero-Canelon, I.; Qamar, B.; Liu, Z.; Hands-Portman, I.; Sadler, P. J. Organometallic iridium(III) anticancer complexes with new mechanisms of action: NCI-60 screening, mitochondrial targeting, and apoptosis. *ACS Chem. Biol.* **2013**, *8*, 1335−1343. (d) Starha, P.; Trávníček, Z.; Drahoš, B.; Herchel, R.; Dvořák, Z. Cell-based studies of the first-in-class half-sandwich Ir(III) complex containing histone deacetylase inhibitor 4-phenylbutyrate. *Appl. Organomet. Chem.* **2018**, *32*, e4246.

(25) (a) Zanoni, M.; Piccinini, F.; Arienti, C.; Zamagni, A.; Santi, S.; Polico, R.; Bevilacqua, A.; Tesei, A. 3D tumor spheroid models for in vitrotherapeutic screening: a systematic approach to enhance the biological relevance of data obtained. *Sci. Rep.* **2016**, *6*, 19103. (b) Thoma, C. R.; Zimmermann, M.; Agarkova, I.; Kelm, J. M.; Krek, W. 3D cell culture systems modeling tumor growth determinants in cancer target discovery. *Adv. Drug Delivery Rev.* **2014**, *69*−*70*, 29−41.

(26) (a) Baker, B. M.; Chen, C. S. Deconstructing the third dimension − how 3D culture microenvironments alter cellular cues. *J. Cell Sci.* **2012**, *125*, 3015−3024. (b) Wartenberg, M.; Ling, F. C.; Müschen, M.; Klein, F.; Acker, H.; Gassmann, M.; Petrat, K.; Pütz, V.; Hescheler, J.; Sauer, H. Regulation of the multidrug resistance transporter P-glycoprotein in multicellular tumor spheroids by hypoxia-inducible factor (HIF-1) and reactive oxygen species. *FASEB J.* **2003**, *17*, 503−505. (c) Minchinton, A. I.; Tannock, I. F. Drug penetration in solid tumours. *Nat. Rev. Cancer* **2006**, *6*, 583−592. (d) Kimlin, L. C.; Casagrande, G.; Virador, V. M. In vitro three-

DOI: 10.1021/acs.organomet.8b00415
Organometallics XXXX, XXX, XXX−XXX

dimensional (3D) models in cancer research: An update. *Mol. Carcinog.* **2013**, *52*, 167−182.
(27) (a) Friedrich, J.; Seidel, C.; Ebner, R.; Kunz-Schughart, L. A. Spheroid-based drug screen: considerations and practical approach. *Nat. Protoc.* **2009**, *4*, 309−324. (b) Jaganathan, H.; Gage, J.; Leonard, F.; Srinivasan, S.; Souza, G. R.; Dave, B.; Godin, B. Three-dimensional in vitro co-culture model of breast tumor using magnetic levitation. *Sci. Rep.* **2015**, *4*, 6468.
(28) Łakomska, I.; Hoffmann, K.; Wojtczak, A.; Sitkowski, J.; Maj, E.; Wietrzyk, J. Cytotoxic malonate platinum(II) complexes with 1,2,4-triazolo[1,5-*a*]pyrimidine derivatives: Structural characterization and mechanism of the suppression of tumor cell growth. *J. Inorg. Biochem.* **2014**, *141*, 188−197.
(29) Ossipov, K.; Scaffidi-Domianello, Y. Y.; Seregina, I. F.; Galanski, M.; Keppler, B. K.; Timerbaev, A. R.; Bolshov, M. A. Inductively coupled plasma mass spectrometry for metallodrug development: Albumin binding and serum distribution of cytotoxic *cis*- and *trans*-isomeric platinum(II) complexes. *J. Inorg. Biochem.* **2014**, *137*, 40−45.
(30) Novohradsky, V.; Zerzankova, L.; Stepankova, J.; Kisova, A.; Kostrhunova, H.; Liu, Z.; Sadler, P. J.; Kasparkova, J.; Brabec, V. A dual-targeting, apoptosis-inducing organometallic half-sandwich iridium anticancer complex. *Metallomics* **2014**, *6*, 1491−1501.
(31) Xiang, H.; Chen, H.; Tham, H. P.; Phua, S. Z. F.; Liu, J. G.; Zhao, Y. Cyclometalated iridium(III)-complex-based micelles for glutathione-responsive targeted chemotherapy and photodynamic therapy. *ACS Appl. Mater. Interfaces* **2017**, *9*, 27553−27562.
(32) Tönnemann, J.; Risse, J.; Grote, Z.; Scopelliti, R.; Severin, K. Efficient and rapid synthesis of chlorido-bridged half-sandwich complexes of ruthenium, rhodium, and iridium by microwave heating. *Eur. J. Inorg. Chem.* **2013**, *2013*, 4558−4562.
(33) Gottlieb, H. E.; Kotlyar, V.; Nudelman, A. NMR chemical shifts of common laboratory solvents as trace impurities. *J. Org. Chem.* **1997**, *62*, 7512−7515.
(34) *Apex3*; Bruker AXS Inc.: Madison, WI, 2015.
(35) Sheldrick, G. M. Crystal structure refinement with SHELXL. *Acta Crystallogr., Sect. C: Struct. Chem.* **2015**, *71*, 3−8.
(36) Brandenburg, K. *Diamond Version 4.0.3*; Crystal Impact GbR: Bonn, Germany, 2015.
(37) Macrae, C. F.; Bruno, I. J.; Chisholm, J. A.; Edgington, P. R.; McCabe, P.; Pidcock, E.; Rodriguez-Monge, L.; Taylor, R.; van de Streek, J.; Wood, P. A. Mercury CSD 2.0 - new features for the visualization and investigation of crystal structures. *J. Appl. Crystallogr.* **2008**, *41*, 466−470.
(38) Salemi, G.; Gueli, M. C.; D'Amelio, M.; Saia, V.; Mangiapane, P.; Aridon, P.; Ragonese, P.; Lupo, I. Blood levels of homocysteine, cysteine, glutathione, folic acid, and vitamin B12 in the acute phase of atherothrombotic stroke. *Neurol. Sci.* **2009**, *30*, 361−364.

DOI: 10.1021/acs.organomet.8b00415
Organometallics XXXX, XXX, XXX−XXX